International Journal of Mechanics and Energy (IJME)
Vol. 1, Issue 1, 2013, ISSN: 2286-5845

Incidence angle effect on the aerodynamic structure of a Savonius wind rotor

Makram Maaloul*, Zied Driss, Mohamed Salah Abid

Laboratory of Electro-Mechanic Systems (LASEM), National School of Engineers of Sfax (ENIS), University of Sfax (US), B.P. 1173, Road Soukra, km 3.5, 3038 Sfax, TUNISIA

Received December 25, 2012 / Accepted May 14, 2013

Abstract: The study of the incidence angle effect around a Savonius wind rotor on the numerical results was obtained using "SolidWorks Flow Simulation" softaware. The objective of this study is to observe the effect of the incidence angle on the aerodynamic structure characteristics. These results are presented in different transverse and longitudinal planes of the considered control volume. To validate the numerical results, we have developed an experimental approach to measure the flow velocity in different positions of the test vein of our wind tunnel.

Key words: Savonius rotor, wind tunnel, incidence angle, aerodynamic structure.

1. Introduction

The Savonius rotor is a vertical axis wind turbine. The rotor is used in many applications, such as water pumping and electricity generation. Several studies have investigated the influence of geometric and aerodynamic parameters of rotor Savonius. For example, Mohamed et al. [1] studied several shapes of obstacles and deflectors placed in front of two and three blade Savonius turbine. A rounded deflector structure was placed in front of two counter-rotating GW-turbines. They studied the effect of an obstacle shielding partly the returning blade of a Savonius turbine as well as a combination of an obstacle and a deflector was numerically investigated for both two and three blade Savonius rotor. An experimental investigation was carried out by Golecha et al. [2] to identify the position of the deflector plate to yield higher coefficient of power for single stage modified Savonius rotor. Akwa et al. [3] reported that the optimum size for the buckets overlap is equal to 15% of the buckets chord size. In addition, Saha and Rajkumar [4] performed work on twist bladed metallic Savonius rotor and compared the performance with conventional semi-circular blades having no twist. They obtained an efficiency of 0.14. Their rotor also produced good starting torque and larger rotational speeds. Kamoji et al. [5] reported that the modified semicircular rotor with an aspect ratio of 0.7 has a maximum coefficient of power. Maximum coefficient of power for a helical Savonius rotor without shaft is around 0.175 for a zero overlap ratio at a tip speed ratio of around 0.9 and at a Reynolds number of 150,000. Influence of Reynolds number was investigated for a modified Savonius rotor (without shaft) for an overlap ratio of zero, aspect ratio of 0.7, blade arc angle of 124°, blade shape factor of 0.2. As a result, the power coefficient increases by 19% as Reynolds number increases from 80,000 to 150,000. Maximum coefficient of power increases with the increase of the Reynolds number. Zhanzhou et al. [6] studied the effect of number of blades on the performance of Savonius rotor. Simulation has been conducted by varying the number of blades from two to three in single stage rotor systems. Both the bigger downwind surface and the smaller upwind surface lead to the better rotor performance. So, the performance of

*** Corresponding author:** Makram Maaloul
E-mail: maaloul.makram@gmail.com

two-bladed rotor is better than that of the three. Menet et al. [7] made systematic calculation to evaluate the influence of the Reynolds number for the optimal rotor. The calculation has been made at the nominal working point λ=1.0 and for θ = 90°. The study shows that the influence of the Reynolds number on the torque coefficient and the power coefficient is always lower than 3% in the studied range of Reynolds numbers (10^5 < Re < 5 10^5). According to these results, it has been showen that the study of the Savonius wind rotor is very important. For these reasons, we are interested to study the incidence angle effect on the aerodynamic structure of a Savonius wind rotor.

2. Geometric system

2.1 Wind tunnel

Figure 1 shows the wind tunnel in which the experiments were conducted. An open type tunnel is used; it is equipped with an aspirator that ensures a stable and uniform air flow. The rotor is placed in the test section to take the experimental values. The total length of the wind tunnel is 3857 mm. the test section is about 400 mm of width, 800 mm of length and 400 mm of height.

Fig. 1 Wind tunnel

2.2 Savonius rotor

The rotor handled in this work is a simple Savonius rotor composed of two halves of cylinder; each one is about 200 mm of height, 100 mm of diameter and 1.5 mm of thickness (figure 2). The fixation element's width is of 24 mm. The primary overlap considered is 20 mm and the secondary overlap is of 10 mm.

Fig. 2 Savonius wind rotor

3. Numerical results

In this paper, the numerical results have been visualized and commented using the "SolidWorks Flow Simulation" softaware. A simulation of the aerodynamics aspects due to the variation of the incidence angle θ is realized. In this section, different values of θ are considered θ=0°, θ=30°, θ=60°, θ=90°, θ=120° and θ=150° (Figure 3). Practically, we are interested to the velocity field, the average velocity, the static pressure, the turbulent kinetic energy, the turbulent dissipation rate, the turbulent viscosity and the vorticity. Three planes defined by x=0 mm, y=0 mm and z=0 mm were considered (figure 4).

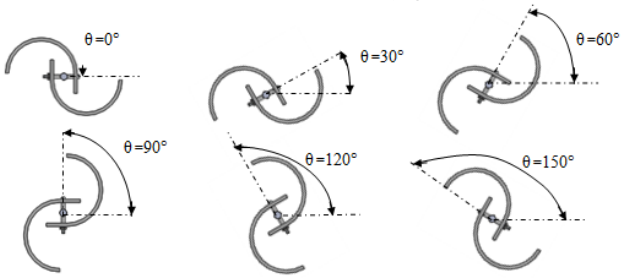

Fig. 3 Incidence angles

3.1 Velocity field

Figures 4 and 5 show the distribution of the velocity field respectively on the planes defined by y=0 mm and z=0 mm. According to these results, the velocity field in the tunnel intake is uniform. It increases gradually with the decrease of the tunnel section. Upstream of the rotor, a deceleration of the velocity has been noted in the region located in the concave surface of the rotor. An acceleration of the velocity has been noted in the region located in the concave surface of the rotor for the incidence angles equal to θ=0°, θ=30°, θ=120° and θ=150°. Downstream of the rotor, a rapid deceleration has been observed. This can be explained by the fact that the rotor can be considered as an obstacle in front of the air flow. Otherwise, there are two recirculation zones at the upper and lower buckets. For θ=0°, a large recirculation zone is formed in the lower buckets. When the incidence angle θ increases, other training recirculation zones in the upper buckets has been noted for the incidence angles equal to θ=30°, θ=60° and θ=90°. For θ=90 °, it is found that there is loss of the recirculation zone at the lower buckets. This fact has been observed also for the incidence angles equal to θ=120° and θ=150 °.

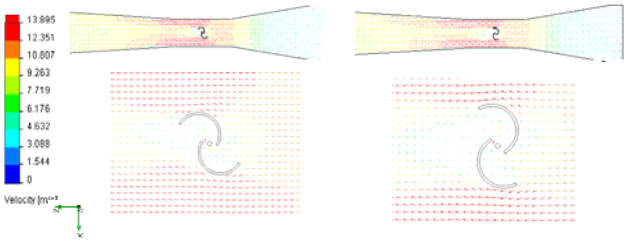

(a) θ=150° (b) θ=120°

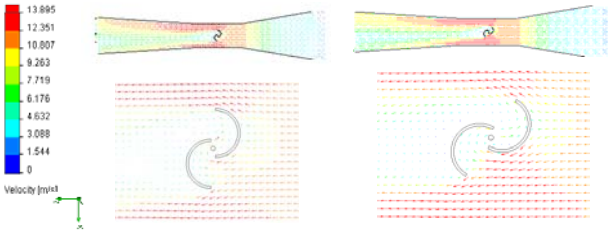

(c) θ=90° (d) θ=60°

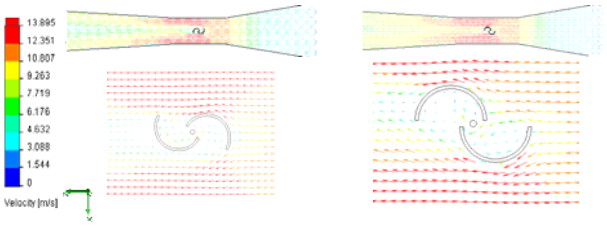

(e) θ=30° (f) θ=0°

Fig. 4 Velocity field on the plane defined by y=0 mm

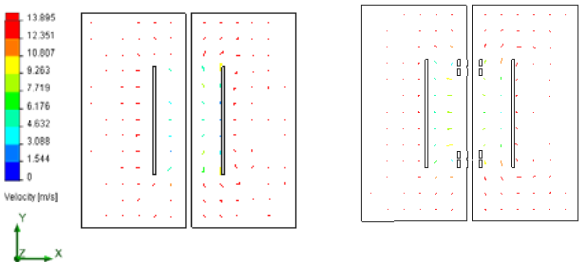

(a) θ=150° (b) θ=120°

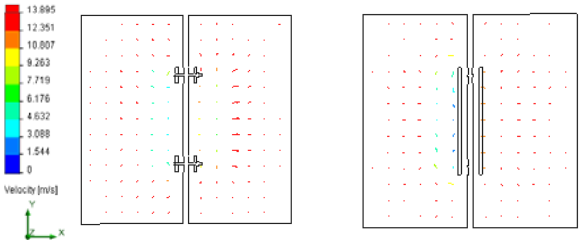

(c) θ=90° (d) θ=60°

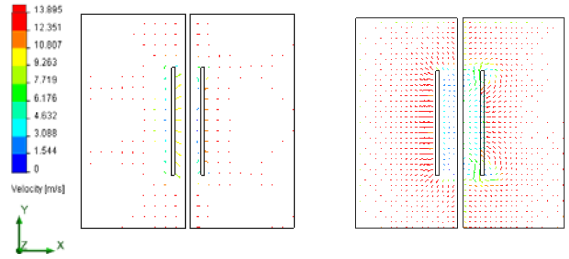

(e) θ=30° (f) θ=0°

Fig. 5 Velocity field on the plane defined by z=0 mm

3.2. Average velocity

Figures 6 and 7 show the distribution of the average velocity on the planes defined respectively by y=0 mm and z=0 mm. The velocity in the tunnel intake is uniform. It increases gradually with the decrease of the tunnel section. Upstream of the rotor, a deceleration of the velocity has been noted in the

region located in the concave surface of the rotor. In the other hand, a rapid deceleration downstream of the rotor has been observed. This can be explained by the fact that the rotor can be considered as an obstacle in front of the air flow that captures the turbulent kinetic energy of the wind. For θ=0°, θ=120° and θ=150°, a wake characteristic of the maximum velocity values is located in the convex surface of the two buckets. The maximum velocity value is located on the upper and lower buckets edge's for θ=60°, θ=90° and θ=120°. Indeed, two wakes are formed in the downstream of the rotor where the minimum velocity values are recorded. For the incidence angles equals to θ=0°, θ=120° and θ=150°, a symmetric distribution has been observed. However, for θ=60°, θ=90° and θ=30° a dissymmetric distribution has been noted.

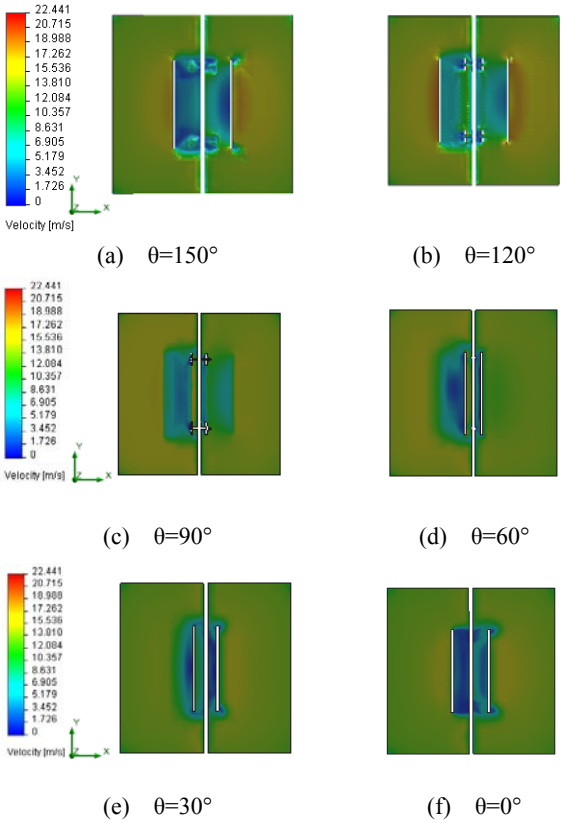

(a) θ=150° (b) θ=120°

(c) θ=90° (d) θ=60°

(e) θ=30° (f) θ=0°

Fig. 6 Distribution of the average velocity on the plane defined by z=0 mm

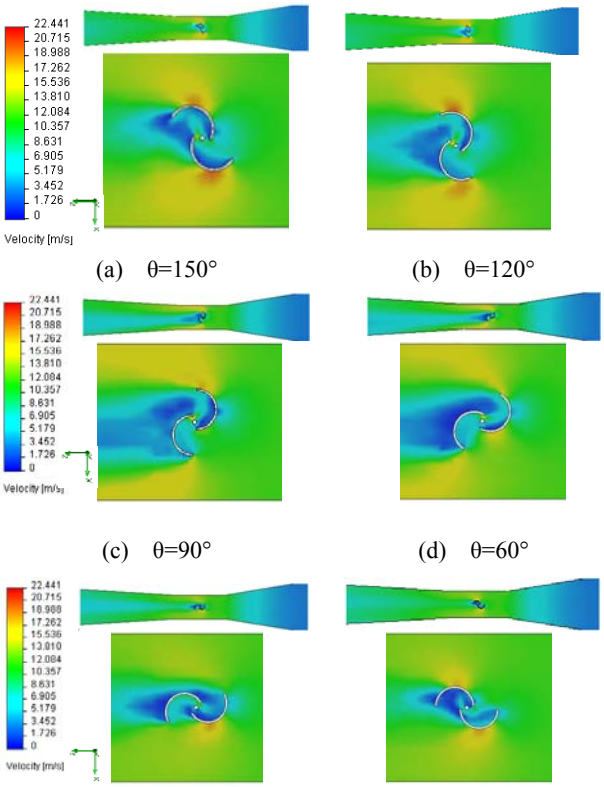

(a) θ=150° (b) θ=120°

(c) θ=90° (d) θ=60°

(e) θ=30° (f) θ=0°

Fig. 7 Distribution of the average velocity on the plane defined by y=0 mm

3.3. Static pressure

Figures 8 and 9 show the distribution of the static pressure on the planes defined respectively by y=0 mm and z=0 mm. According to these results, the pressure is globally uniform in the wind tunnel upstream. In the downstream, a weak depression zone appears for θ=150° and θ=120°. These zones become more large for θ=60° and θ=90°. The largest area of pressure appears for the incidence angles equal to θ=150°, θ=120° and θ=90°. The largest area of depression appears for the incidence angles equals to θ=60°, θ=30° and θ=0°. The compression zone appears for θ=150°, θ=120° and θ=90° and less important for θ=60°. For θ=90°, the rotor configuration is allowing it to play the role of a large obstacle and the static pressure is high in the collector and in the upstream of the rotor. A rapid decrease in

the static pressure in the downstream of the rotor causes a depression zone and the total pressure keeps increasing in the way out of the wind tunnel.

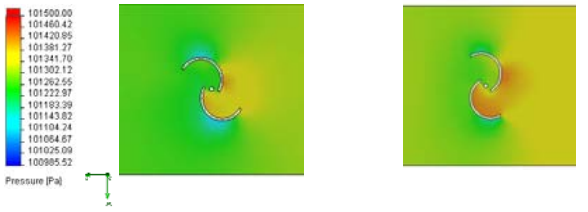

(a) θ=150° (b) θ=120°

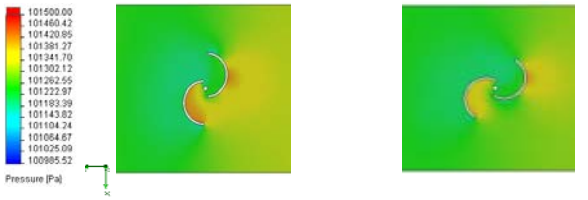

(c) θ=90° (d) θ=60°

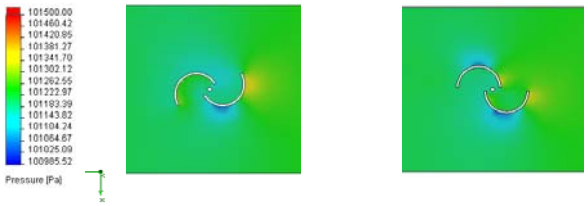

(e) θ=30° (f) θ=0°

Fig. 8 Distribution of the static pressure on the plane defined by y=0 mm

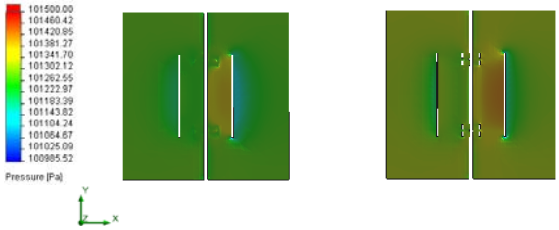

(a) θ=150° (b) θ=120°

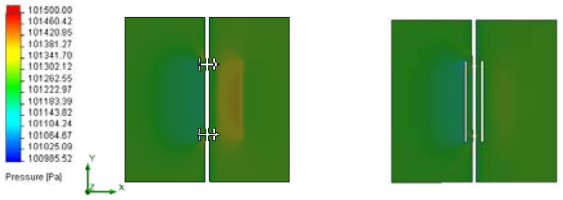

(c) θ=90° (d) θ=60°

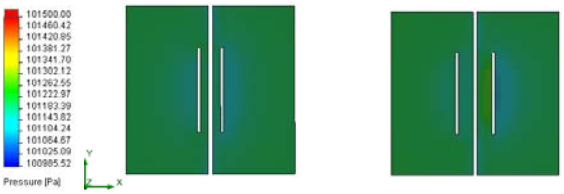

(e) θ=30° (f) θ=0°

Fig. 9 Distribution of the static pressure on the plane defined by z=0 mm

3.4. Vorticity

Figures 10 and 11 show the distribution of the vorticity on the planes defined respectively by y=0 mm, and z=0 mm. According to these results, it has been noted that the vorticity is very weak out of the test vein for all the values of the incidence angles. Indeed, it increases around the rotor and in the rotor downstream.

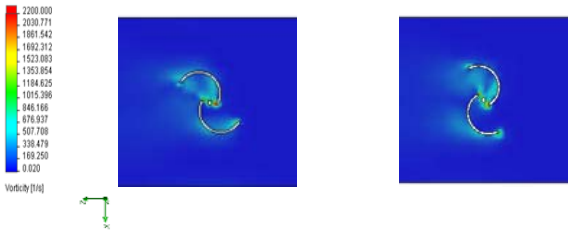

(a) θ=150° (b) θ=120°

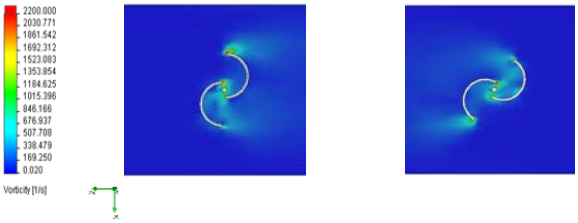

(c) θ=90° (d) θ=60°

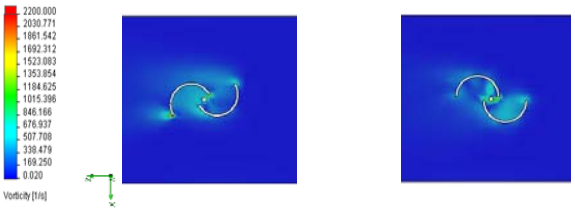

(e) θ=30° (f) θ=0°

Fig. 10 Distribution of the vorticity on the plane defined by y=0 mm

For θ=150°, θ=120° and θ=0°, the vorticity get its maximum in the internal leading edges of two buckets. The vorticity reaches its maximum in the leading external edges of the two buckets for θ=90°, θ=60° and θ=30°.

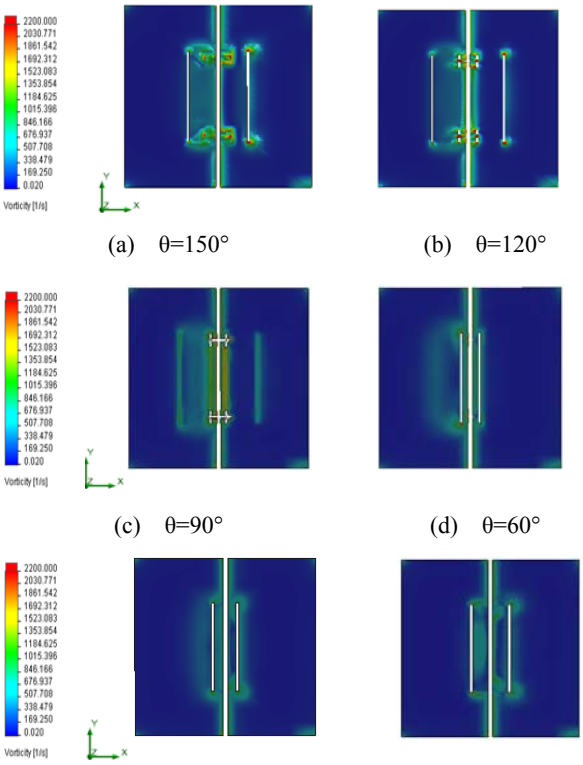

(a) θ=150° (b) θ=120°

(c) θ=90° (d) θ=60°

(e) θ=30° (f) θ=0°

Fig. 11 Distribution of the vorticity on the plane defined by z=0 mm

3.5. Turbulent kinetic energy

Figures 12 and 13 show the distribution of the turbulent kinetic energy on the planes defined respectively by y=0 mm and z=0 mm. The maximum turbulent kinetic energy values are recorded in the internal and external leading of the two buckets for the incidence angles equal to θ=150°, θ=120°, θ=90° and θ=60 °. For θ=0° and θ=30°, a wake zone characteristic of the minimum values appears in the concave surface of the upper buckets. The maximum value is located in the convex surface of the two buckets for the incidence angles equals to θ=150 °, θ=120 ° and θ=0 °.

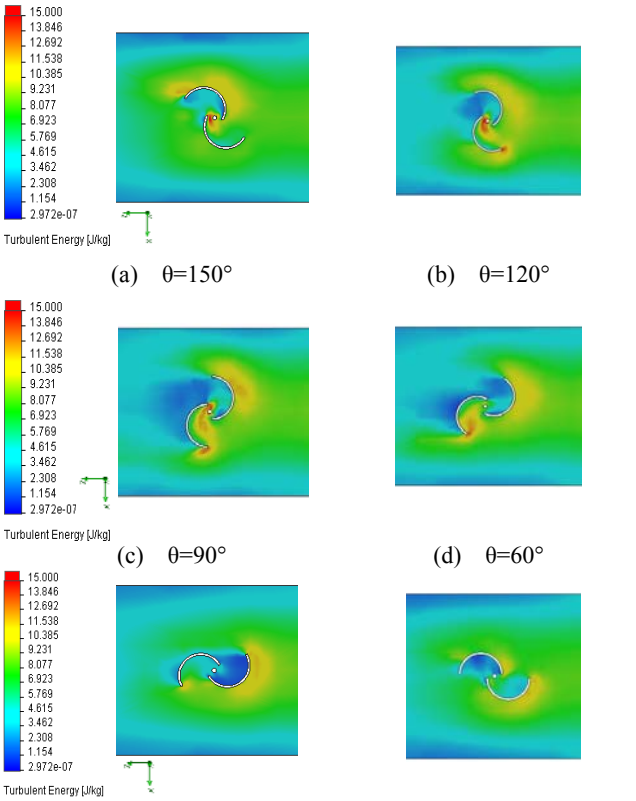

(a) θ=150° (b) θ=120°

(c) θ=90° (d) θ=60°

(e) θ=30° (f) θ=0°

Fig. 12 Distribution of the turbulent kinetic energy on the plane defined by y=0 mm

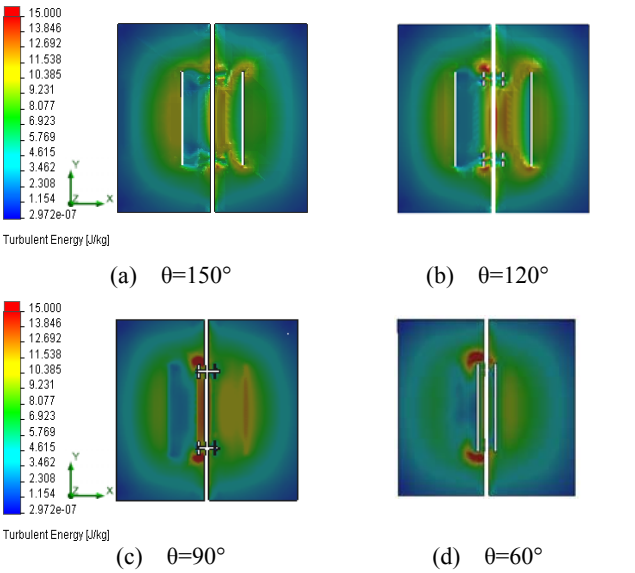

(a) θ=150° (b) θ=120°

(c) θ=90° (d) θ=60°

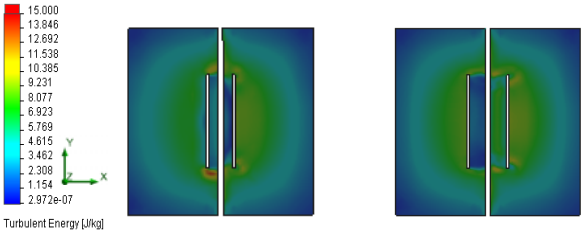

(e) θ=30° (f) θ=0°

Fig. 13 Distribution of the turbulent kinetic energy on the plane defined by z=0 mm

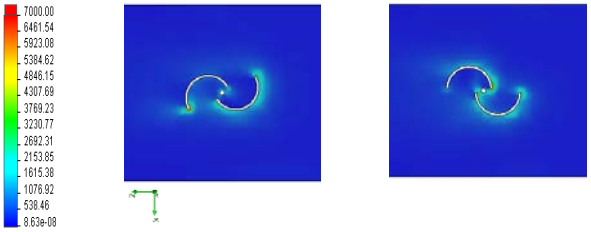

(e) θ=30° (f) θ=0°

Fig.14 Distribution of the turbulent dissipation rate on the plane defined by y=0 mm

3.6. Turbulent dissipation rate

Figures 14 and 15 show the distribution of turbulent dissipation rate on the planes defined respectively by y=0 mm and z=0 mm. The maximum turbulent dissipation rate value is located in the convex surface of the two buckets. The maximum values are recorded in the leading of the two buckets for the incidence angles equal to θ=150°, θ=120°, θ=90°, θ=60° and θ=0°. A rapid decrease of the turbulent dissipation rate appears in the downstream of the rotor.

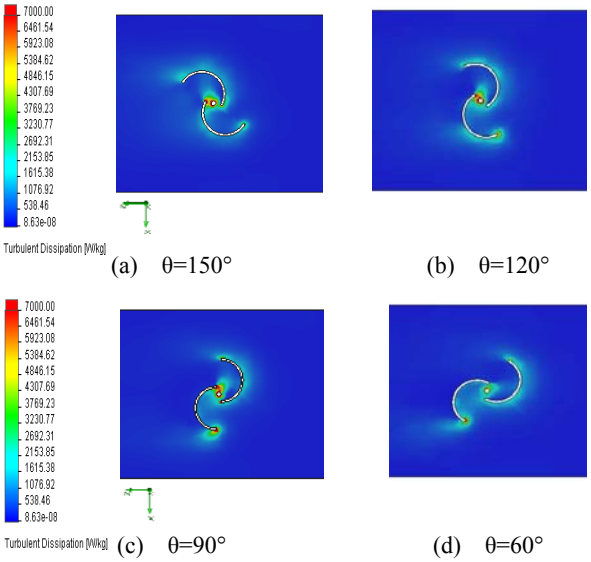

(a) θ=150° (b) θ=120°

(c) θ=90° (d) θ=60°

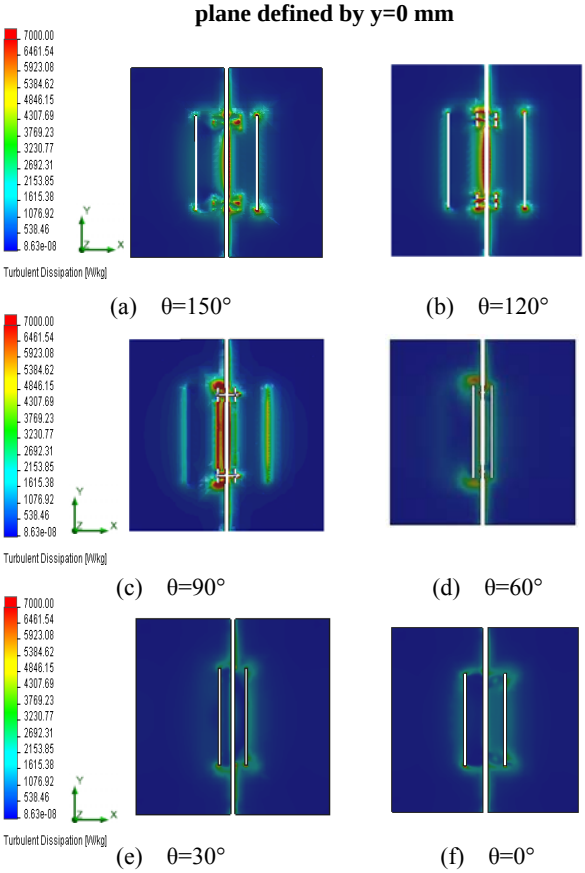

(a) θ=150° (b) θ=120°

(c) θ=90° (d) θ=60°

(e) θ=30° (f) θ=0°

Fig. 15 Distribution of the turbulent dissipation rate on the plane defined by z=0 mm

3.7. Turbulent viscosity

Figures 16 and 17 show the distribution of the turbulent viscosity on the planes defined respectively by y=0 mm and z=0 mm. Based on these results, it has been noted that the value of the turbulent viscosity is high in the tunnel Intel. However, in the rotor upstream, this value decreases abruptly. Moreover, we find that the incidence angle has a direct affect on the distribution of turbulent viscosity. The wake zone

characteristic of the maximum values of the turbulent viscosity appears in the inlet and extends to meet the Savonius rotor. This phenomenon has been observed for the incidence angles equal to θ=150°, θ=120°, θ=90° and θ=60°. However, for the incidence angles equals to θ=30 ° and θ=0 °, the wake zone extends just in the upstream of the Savonius rotor. In addition, a wake zone characteristic of the minimum values seats on the concave surface of the upper buckets. This wake zone extends on the lower buckets.

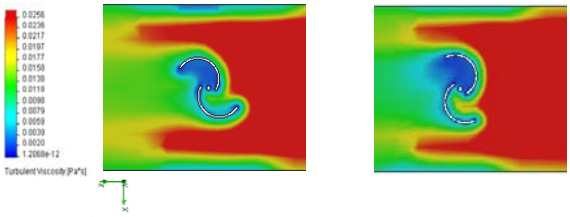

(a) θ=150° (b) θ=120°

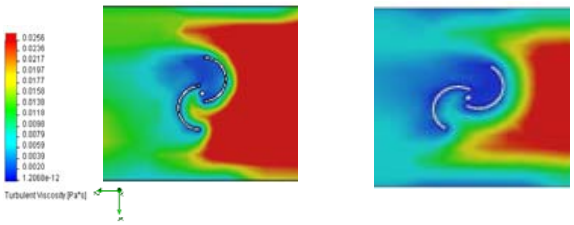

(c) θ=90° (d) θ=60°

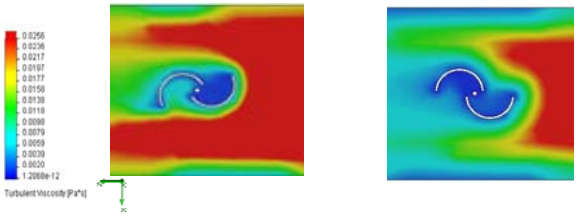

(e) θ=30° (f) θ=0°

Fig.16 Distribution of the turbulent viscosity on the plane defined by y=0 mm

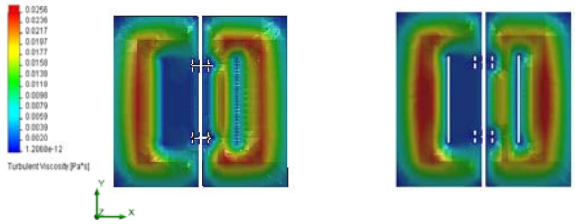

(a) θ=150° (b) θ=120°

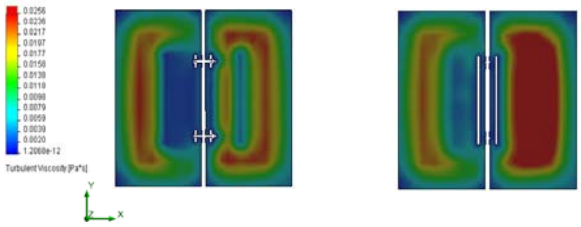

(c) θ=90° (d) θ=60°

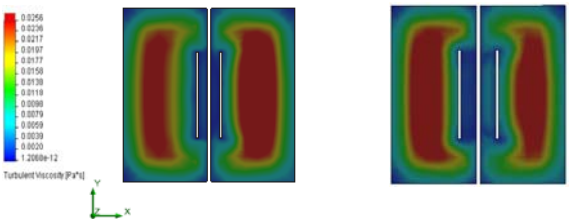

(e) θ=30° (f) θ=0°

Fig.17 Distribution of the turbulent viscosity on the plane defined by z=0 mm

4. Comparison with experimental results

For the validation of the numerical results, we are interested in determining of the average speed profiles for x=0 mm in different transverse planes defined by the positions z=-50 mm and z=150 mm (Figure 18). This is done by positioning the probe of the anemometer for each point and to take the value of the displayed speed air flow. By comparing these profiles from one position to another, we see that all the experimental curves have similar gaits resembling digital. This proves the validity of the numerical method.

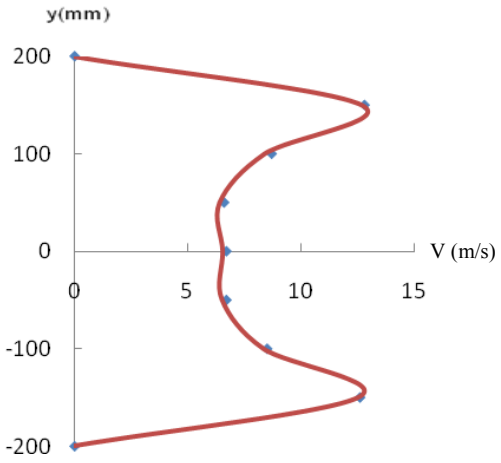

(a) Z=-50 mm

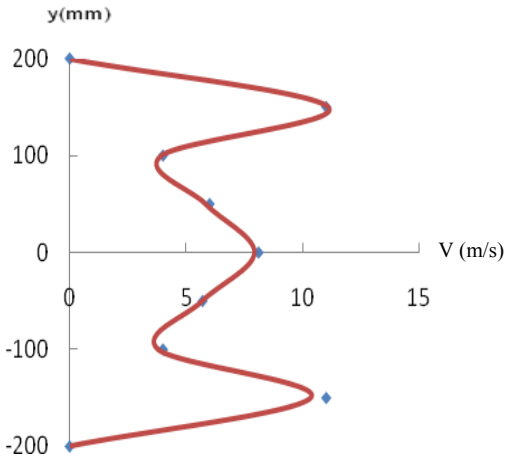

(b) Z=150 mm

Fig.18 Average speed profiles

5. Conclusion

In this paper, we have studied numerically the aerodynamic structure around the Savonius wind rotor. This study is done using the softaware "SolidWorks Flow Simulation". The code used for the numerical simulation allowed us to deepen the knowledge of the aerodynamic behavior of the wind rotor. Particularly, we are interested in studying of the incidence angle effect of the Savonius rotor. For these configurations, the aerodynamic structure characteristics are presented in different transverse and longitudinal planes of the considered control volume. From these results, we conclude that the speed grows up with the increase of the incidence angle. Depression areas tend to be more developed in the case of the smaller incidence angle.

In the future, we propose to develop a PIV study for a finer knowledge of the aerodynamic characteristics.

6. References

[1] M.H. Mohamed, G. Janiga, E. Pap, D. Thévenin, Optimal blade shape of a modified Savonius turbine using an obstacle shielding the returning blade. Energy Conversion and Management 52 (2011) 236–242.

[2] K. Golecha, T.I. Eldho, S.V. Prabhu, Influence of the deflector plate on the performance of modified Savonius water turbine. Applied Energy 88 (2011).

[3] J.V. Akwaa, H.A. Vielmob, A.P. Petryb, A review on the performance of Savonius wind turbines. Renewable and Sustainable Energy Reviews 16 (2012) 3054– 3064.

[4] U.K. Saha, M. Jaya Rajkumar, On the performance analysis of Savonius rotor with twisted blades, Renewable Energy 31 (2006) 1776-1788.

[5] M.A. Kamoji, Kedare S.B., Prabhu S.V. Performance tests on helical Savonius rotors. Renewable Energy 34 (2009) 521–529.

[6] Z. Zhenzhou, Z. Yuan, X. Xiaoyun, Wenming, L. Guoxiang H. Research on the Improvement of the Performance of Savonius Rotor Based on Numerical Study, 2008.

[7] J.L. Menet, N. Bourabaa, Increase in the Savonius rotors efficiency via a parametric investigation. European Wind Energy Conference, London, 2004.